

Published in final edited form as:

Int J Pharm. 2012 November 15; 438(0): 140–149. doi:10.1016/j.ijpharm.2012.08.026.

## FLUX OF IONIC DYES ACROSS MICRONEEDLE-TREATED SKIN: EFFECT OF DYE MOLECULAR CHARACTERISTICS

Yasmine A. Gomaa<sup>a,c</sup>, Martin J. Garland<sup>b</sup>, Fiona McInnes<sup>a,1,\*</sup>, Ryan F. Donnelly<sup>b</sup>, Labiba K. El-Khordagui<sup>c</sup>, and Clive Wilson<sup>a</sup>

<sup>a</sup>Strathclyde Institute of Pharmacy and Biomedical Sciences (SIPBS), University of Strathclyde, 161 Cathedral Street, Glasgow, G4 0RE Scotland, UK.

<sup>b</sup>School of Pharmacy, Queen's University of Belfast, 97 Lisburn Road, Belfast, BT9 7BL, Northern Ireland, UK.

<sup>c</sup>Department of Pharmaceutics, Faculty of Pharmacy, Alexandria University, El-Khartoum square, Alexandria, 21521, Egypt.

<sup>1</sup>Drug Delivery International, Bio-Imaging Centre, Basement Medical Block, Within Glasgow Royal Infirmary, 84 Castle Street, Glasgow G4 0SF, UK.

### Abstract

Drug flux across microneedle (MN)-treated skin is influenced by the characteristics of the MN array, microconduits and drug molecules in addition to the overall diffusional resistance of microconduits and viable tissue. Relative implication of these factors has not been fully explored. In the present study, the *in vitro* permeation of a series of six structurally related ionic xanthene dyes with different molecular weights (MW) and chemical substituents, across polymer MN-pretreated full thickness porcine skin was investigated in relation of their molecular characteristics. Phosphate buffer saline pH 7.4, the medium used in skin permeation experiments, was used to determine the equilibrium solubility of the dyes and their partition coefficient both in the isotropic n-octanol/ aqueous system and porcine skin/ aqueous system. Additionally, dissociation constants were determined potentiometrically. Results indicated that for rhodamine dyes, skin permeation of the zwitterionic form which predominates at physiological pH, was significantly reduced by an increase in MW, the presence of the chemically reactive isothiocyanate substituent reported to interact with *stratum corneum* proteins and the skin thickness. These factors were generally shown to override aqueous solubility, an important determinant of drug diffusion in an aqueous milieu. Findings provided more insight into the mechanism of drug permeation across MN-treated skin, of importance to both the design of MN-based transdermal drug delivery systems and *in vitro* skin permeation research.

### Keywords

microneedles; molecular weight; solubility; porcine skin; isothiocyanate; partition coefficient

---

\*Corresponding author: Fiona McInnes .

## Introduction

Microneedle (MN) arrays were developed over the past two decades as a novel physical enhancement means and/or drug carrier for the dermal and transdermal delivery of drugs with poor oral bioavailability or percutaneous absorption<sup>(1)</sup>. By piercing the *stratum corneum* (SC), the primary barrier to percutaneous absorption, MN create transient SC-independent aqueous microconduits as multiple pathways, particularly for hydrophilic drugs, to the aqueous milieu of viable tissues<sup>(2)</sup>. This brings into play determinants of transdermal drug delivery, different from those primarily controlling percutaneous absorption such as low molecular weight (MW), lipophilicity and potency<sup>(3)</sup>.

In MN-treated skin, a molecule needs to diffuse through the aqueous microchannels and traverse several layers of the viable tissue in series to reach the receiver compartment of the diffusion cell in the *in vitro* setup or to the dermal vasculature *in vivo*<sup>(2)</sup>. In *in vitro* skin permeation experiments, the mainstay of MN-based research, this multifactorial process can be significantly affected by the interplay of variables relating to technological features of MN arrays, characteristics of the MN-created microconduits, the experimental setup and the drug molecular characteristics.

MN array technological features, mainly chemical composition, configuration, MN geometry and the approach used for drug delivery to the skin, proved to play a main role in MN-enhanced transdermal drug delivery<sup>(4)</sup>. Such features have been greatly enhanced by major technological advances achieved in the design and fabrication of MN arrays<sup>(5, 6)</sup>.

Characteristics of MN-created microconduits, in terms of dimensions and geometry in addition to their relatively short lifetime duration<sup>(7)</sup> contribute to the overall diffusional resistance to drug transport<sup>(2)</sup>.

Further, characteristics of *ex vivo* skin samples including type<sup>(8)</sup> and thickness<sup>(9)</sup> have been implicated in the quality of MN-based drug delivery data. Although full thickness skin provides a closer simulation of the *in vivo* setting, it reduces flux values by approximately five orders of magnitude<sup>(10)</sup>.

Among factors affecting drug transport through MN-treated skin, drug formulation variables including drug molecular characteristics<sup>(11, 12)</sup> and formulation either in an isotropic solution system<sup>(2)</sup> or drug-loaded nanocarriers<sup>(13-15)</sup> has been the least explored.

The aim of this study was to investigate the *in vitro* skin permeation of a series of structurally related xanthene dyes across MN-treated skin in relation to their molecular characteristics. To this end, six structurally related ionic xanthene dyes with a wide range of MW and different chemical substituents were selected for transport across intact and MN-treated full thickness porcine ear skin at physiological pH. These dyes were selected being the most widely used fluorophores in fluorescence-based diagnostic and imaging applications<sup>(16, 17)</sup> and easily determined spectrofluorometrically<sup>(18)</sup>. MN-treated skin permeation data of the dyes were interpreted in relation to their passive diffusion data and physicochemical properties determined using phosphate buffer saline (PBS) pH 7.4.

## Material and methods

### Materials

Rh 110 (MW 366.8 Da), Rh B (MW 479.02 Da), RITC (MW 536.08 Da), RITC-D (MW 10 KDa), TRITC-D (MW 4400 Da), and FITC (MW 389.38 Da), PBS tablets (pH 7.4), potassium chloride (KCl), potassium hydroxide (KOH), hydrochloric acid (HCl), methanol, ethanol, and n-octanol, were obtained from Sigma-Aldrich (St. Louis, MO, USA). Dyes were used without further purification. Gantrez® AN-139, a copolymer of methylvinylether co-maleic anhydride (PMVE/MA), was provided by ISP Co. 120 Ltd. (Guildford, UK). Silastic® 9280/60E silicone elastomer was purchased from Dow Corning (Midland, MI, USA). ‘Silver dag’- colloidal silver - was purchased from Polysciences Inc. (Eppelheim, Germany). Shandon M-1 embedding OCT (optimal cutting temperature) matrix was bought from Thermo Electron Corporation, UK.

### Methods

A series of six structurally-related ionic xanthene dyes were selected for the study. The dyes are physicochemical diverse and covering a wide range of MW (366.80 Da to 10 KDa). Chemical structures of the selected dyes are shown in Figure 1.

### Physicochemical characterization of the dyes

**Determination of the dissociation constants (pKa) of the dyes**—An automated pKa analyser (Sirius T3 apparatus, Sirius Analytical Instruments Ltd, Forest Row, East Sussex, RH18 5DW, UK) at a temperature of  $25^{\circ}\text{C} \pm 0.5^{\circ}\text{C}$  fitted with a Ag/AgCl double junction reference electrode, was used for the determination of the dyes pKa. Potentiometric pKa titrations were carried out under an Argon atmosphere in ion strength-adjusted water (0.15 M KCl) using either 0.5 M KOH or 0.5 M HCl as titrants. Triplicate titrations were performed over the pH range 2 to 12. Whenever needed, cosolvent mixtures of ethanol or methanol in 0.15 M KCl-adjusted water were used to dissolve the dyes. Aqueous pKa values of dyes obtained using cosolvent mixtures was determined from their corresponding cosolvent dissociation constant (psKa) using the Yasuda-Shedlovesky procedure<sup>(19)</sup>. This procedure involves determining the psKa of the dyes in various cosolvent mixtures from which the aqueous pKa can be determined by extrapolation to zero cosolvent concentration.

**Determination of the dyes solubility in PBS**—The solubility of the dyes was determined in PBS (pH 7.4) at  $37^{\circ}\text{C}$  using the flask saturation method<sup>(20)</sup>. An excess amount of the dye was added to 0.3 mL of PBS (pH 7.4) in a 1.5 mL centrifuge tube. The tubes were shaken in a thermostatically controlled water bath (DMS360, Fischer Scientific, Leicestershire, UK) at  $37^{\circ}\text{C}$  for 48 h and finally centrifuged (Hettich Zentrifugen Mikro 200, DJB Labcare, UK) at 10000 rpm for 10 min. The supernatant was analyzed using a Varian Cary Eclipse fluorescence spectrophotometer (Mulgrave, Victoria, Australia) with excitation and emission wavelengths of tested dyes were set at 498/520 nm (Rh 110), 540/625 nm (Rh B), 550/580 nm (RITC), 570/590 nm (RITC-D), 555/580 nm (TRITC-D) and, 495/525 nm (FITC). Data presented are the averages of at least three determinations.

**Determination of pH of dye solutions in PBS**—The pH of 162  $\mu\text{M}$  solution of the test dyes in PBS pH 7.4 used in skin permeation studies was measured using a microprocessor pH meter (Hanna instruments, Leighton Buzzard, UK).

**Determination of the n-octanol / PBS dye partition coefficient ( $K_{O/PBS}$ )**—The n-octanol / PBS dye partition coefficient was determined to estimate the partitioning between SC lipids and aqueous vehicle of the dyes using n-octanol as a similar microenvironment to the anisotropic SC lipids<sup>(2)</sup>. Equal volumes (5 mL) of n-octanol and the dye solutions of equimolar concentration (162  $\mu\text{M}$ ) in PBS (pH 7.4) were placed in screw cap glass vials. For preparation of RITC dye solution, the dye was initially dissolved in the minimal volume of hot water then diluted to the required final concentration using PBS (pH 7.4). The mixtures were shaken in a thermostatically controlled water bath (DMS360, Fischer Scientific, Leicestershire, UK) at 37°C for 24 h. The aqueous phase was separated, centrifuged (Hettich Zentrifugen Mikro 200, DJB Labcare, UK) for 20 min at 2000 rpm and finally assayed spectrofluorometrically as mentioned previously. Experiments were conducted at least in triplicate.  $K_{O/PBS}$  was calculated using the following equation<sup>(21)</sup>:

$$K_{O/PBS} = (C_a - C_{eq}) / C_{eq}$$

Where,  $C_a$  and  $C_{eq}$  are the dye concentration in the aqueous layer at the beginning of the experiment and at equilibrium, respectively.

**Determination of the porcine skin /PBS dye partition coefficient ( $K_{S/PBS}$ )**—The dye partition coefficient between porcine skin and PBS pH 7.4 ( $K_{S/PBS}$ ) was determined as reported by Tojo *et al.*<sup>(22)</sup>. Full thickness porcine skin was obtained from ears of pigs (Landrace species), harvested immediately following slaughter at a local abattoir (Glasgow, UK). The ears were sectioned using a scalpel to yield whole skin samples. The average thickness of skin samples, as measured by a digital micrometer, was  $1164 \pm 103 \mu\text{m}$  ( $n = 46$ ). A full thickness porcine ear section was accurately weighed (90 to 100 mg) and placed in a screw cap glass vial containing 10 mL of equimolar dye solutions (162  $\mu\text{M}$ ) in PBS (pH 7.4). The skin samples were equilibrated in the dye solutions for 24 h at 37°C in a thermostatically controlled water bath (DMS360, Fischer Scientific, Leicestershire, UK). The solution was filtered and the dye content was determined spectrofluorometrically as mentioned previously.  $K_{S/PBS}$  was calculated using the following equation<sup>(23)</sup>:

$$K_{S/PBS} = \frac{C_a - C_{eq}}{C_{eq}} \times \frac{1000}{W_e}$$

Where,  $C_a$ ,  $C_{eq}$ , and  $W_e$  are the initial concentration of the dyes in PBS (mg/mL), equilibrium concentration (mg/mL), and average dry weight of the skin (mg), respectively. Data presented are the average of at least 3 determinations.

## Fabrication and characterization of microneedle (MN) arrays

MN arrays were fabricated using 30% PMVE/MA copolymer (Gantrez® AN-139) and laser-engineered silicon micro-moulding, as described previously<sup>(24)</sup>. Briefly, micro-moulds templates were fabricated by curing silicon elastomer poured into an aluminium mould overnight at 40°C. MN moulds, 600 µm length, 300 µm basal width and 121 MN/array density were fabricated using a laser beam (Coherent Avia, Coherent Inc., Pittsburgh, USA) with a wavelength of 355 nm and a pulse length of 30 ns (variable from 1 to 100 kHz) produced by a laser micromachining system (BluLase® Micromachining System, Blueacre Technology, Dundalk, Ireland). Arrays were fabricated by dispersing the copolymer in ice-cold deionised water, followed by vigorous stirring and heating at 95.0°C until a clear gel was formed. The concentration of the polymer blend solution was readjusted to 30% with deionised water then poured into the silicon micro-moulds, centrifuged for 15 min at 3500 rpm and allowed to dry under ambient conditions for 24 h. MN arrays with a base plate were removed from the micro-moulds.

The prepared MN arrays were viewed by scanning electron microscopy (SEM). The arrays were mounted on aluminium stubs using double-sided adhesive tape and 'silver dag'. A SC515 SEM sputter coater (Polaron, East Grinstead, UK) was used to coat the arrays with a 20 nm-thick layer of gold / palladium. The arrays were observed under a JSM 6400 digital SEM (JEOL Ltd, Tokyo, Japan) and photomicrographs of MN structures were taken.

## *In vitro* permeation studies

Two skin models, full thickness porcine skin and dermatomed human skin (DHS), were used as indicated. Porcine skin was prepared as mentioned under: Determination of the n-octanol / PBS dye partition coefficient ( $K_{O/PBS}$ ). DHS was obtained from full thickness cadaveric human skin samples from the abdominal regions of elderly Caucasian females. Skin samples were purchased from the National Disease Research Interchange (Philadelphia, PA, USA). Ethical and regulatory approval was obtained for the use of human skin samples and for subsequent experimentation. The skins were sectioned using a locally designed electric dermatome to produce 330 µm-thick samples. Both skin types were cut into circular samples with a surface area of ~4 cm<sup>2</sup> and wrapped in aluminium foil and stored at -80 °C for no longer than 6 months. Prior to use, the skins were allowed to thaw to room temperature for 1h.

Skin samples (~ 4 cm<sup>2</sup>) were placed, dermal side down, over a polystyrene foam support. MN arrays were manually pressed onto the center of each skin sample 5 times, and arrays were rotated ~ 90° before each re-insertion. The last insertion of the MN lasted for 2s before retraction of the array. The MN-treated skin samples were then inserted as barrier membranes in the Franz cells (PermeGear, Bethlehem, PA, USA) ensuring that the MN-treated sites were positioned centrally over the 0.64 cm<sup>2</sup> diffusionally-available surface area. Untreated skin samples were used as controls. The receiver cells contained 5.3 mL PBS (pH 7.4), which was stirred at 600 rpm at 37°C. Skin samples were then equilibrated to the diffusion cell conditions for 1 h before application of the dye solutions. The permeation experiment was started by adding a 500 µL aliquot of solutions of equimolar concentrations

(162  $\mu\text{M}$ ) of the six dyes in PBS (pH 7.4). Permeation experiments were conducted under non-occlusive conditions for a 48 h-duration.

In studying the influence of the ionic form of Rh B on permeation through MN treated porcine skin, Rh B aqueous solution (162  $\mu\text{M}$  in PBS 7.4 adjusted to pH 3.2 with 0.1 M HCl) was included. The same procedure was used to assess the effect of skin model (full thickness porcine skin *versus* DHS) on the skin permeation of RITC, RITC-D and TRITC-D. Sink conditions were maintained throughout the study.

In all cases, aliquots of 100  $\mu\text{L}$  were removed from the sampling arm at specific intervals over 48 h (10 aliquots) and were compensated with an equal volume of fresh PBS to maintain a constant volume. The withdrawn samples were assayed spectrofluorometrically. Experiments were run at least in triplicate.

The permeation data were plotted as the cumulative amount of dyes collected in the receiver compartment *versus* time. The intact skin path way flux ( $J_{ISP}$ ) and total flux through MN treated skin ( $J_{TOT}$ ) was calculated by dividing the slope of the linear portion of their time permeation profiles by the diffusional skin area (0.64  $\text{cm}^2$ ). Assuming independence of the intact and microchannel skin pathways and considering the possibility of intact skin permeation of dyes, flux through microchannel pathways ( $J_{MCP}$ ) can be calculated according to the following equation<sup>(2)</sup>:

$$J_{MCP} = J_{TOT} - J_{ISP}$$

Permeability coefficients ( $K_p$ ) were determined by normalizing the  $J_{MCP}$  with the initial concentration of the dye in the donor solution in  $\mu\text{g}/\text{cm}^3$ . The flux enhancement ratio was calculated by dividing the  $J_{MCP}$  by the  $J_{ISP}$ .

### Light microscopy of sectioned skin samples

At the end of permeation experiments involving Rh B, the skin surface was cleaned under running cold water then wiped with a tissue to remove traces of the formulation. The skin section exposed to the formulation (marked pink) was excised using a scalpel. This skin tissue was kept in a Shandon crytome® (SME Cryostat, Fisher Thermo Scientific, Asheville, NC) environment operated at  $-25^\circ\text{C}$  prior to sectioning. Frozen sections were mounted on the sample holder of the crytome® using an OCT matrix. The sample holder was then placed on the crytome® stage so that the slicing direction is perpendicular to the skin surface to yield vertical skin sections of 10  $\mu\text{m}$  in thickness. Photomicrographs of vertical sections of the MN-created microconduits were imaged using a DFC320 camera (Leica Microsystems Wetzlar GmbH, Germany) attached to a DM LB2 light microscope (Leica Microsystems Wetzlar GmbH, Germany). No staining was required.

### Statistical analysis

Where appropriate, a Mann Whitney U and a Kruskal-Wallis test followed by a post hoc Dunn's test were used to analyse *in vitro* permeation data using SPSS software (SPSS Inc., Chicago, IL, USA). In all cases,  $P < 0.05$  denoted significance.

## Results and discussion

Creation of hydrophilic microchannels in the upper skin layers by MN to bypass the SC barrier dramatically changes the mechanism of transdermal drug delivery and the relative importance of physiological and physicochemical parameters involved therein. In microporated skin, the permeant has to traverse a series of layers of hydrophilic viable tissues, driven by concentration gradient, before reaching the dermis microvasculature<sup>(2)</sup>. Accordingly, the diffusional resistance of the SC to drug permeation is replaced to a large extent by the diffusional resistances of the microchannels and the tissues beneath. This renders drug diffusivity both in the microchannel and viable tissue, generally modeled by diffusivity in water<sup>(25)</sup>; a primary determinant of MN-mediated skin permeation. Accordingly, drug permeation through microporated skin under *in vitro* conditions, is expected to be affected by Stokes-Einstein equation parameters (vehicle viscosity, permeant hydrodynamic radius, and temperature) in addition to the relative depth of microchannels, thickness of viable tissue to be traversed and the drug concentration gradient<sup>(2)</sup>.

In the present study, a series of structurally related xanthene dyes were used as model ionic permeants to gain more insight into the effect of molecular characteristics on MN-mediated skin permeation under a given set of experimental conditions. The dyes include five rhodamine derivatives, namely Rh 110 and its diethylamino derivative, Rh B, an isothiocyanate congener, RITC, and two related macromolecular dextran conjugates, RITC-D and TRITC-D in addition to one fluorescein isothiocyanate derivative, FITC. The dyes cover a wide range of MW (366.8 D – 10 KD) and were selected owing to their wide use as easily determined fluorescent probes in biomedical applications including skin drug delivery<sup>(18, 26)</sup>.

### Physicochemical properties of the dyes under study

As phosphate buffered saline (PBS) pH 7.4 was the vehicle used for the delivery of the test dyes to porcine ear skin, saturated solubility and partition coefficients of the dyes were determined in this buffer. Results for physicochemical properties investigated are shown in Table 1.

The pKa values for the aromatic carboxylic group of the five rhodamine dyes, determined potentiometrically in ion strength-adjusted water at 25°C, ranged from 3.25 to 3.97. These values coupled with the pH of the dye solutions in PBS pH 7.4 (7.39 to 7.53) indicated that rhodamine dyes are zwitterionic with a net neutral charge at physiological pH and simultaneously bear a positive charge on the quaternary amine group attached to the xanthene ring and a negative charge on the carboxyl group on the isolated benzene ring<sup>(27, 28)</sup>. The pKa values obtained for Rh B and Rh 110 (3.25 and 3.48 respectively, Table 1), were close to reported values, 3.7 and 4.2 for Rh B<sup>(29, 30)</sup> and 4.3 for Rh 110<sup>(31)</sup>. For FITC, a second pKa value ( $6.20 \pm 0.04$ ) corresponding to the ionization of the phenolic OH was determined beside a pKa for the carboxylic group ( $4.06 \pm 0.24$ ). Thus, the prototropic forms of fluorescein include the cation, the monoanion and the dianion depending on the pH of the medium.

Rh B showed the highest solubility in PBS pH 7.4 at 37°C (0.99 M). Rh 110, lacking a quaternary amine group (Figure 1), was much less soluble (0.06 M). The presence of the hydrophobic isothiocyanate substituent (N=C=S) in the benzene ring significantly reduced the solubility of RITC (practically insoluble) compared to the parent compound Rh B. On the other hand, conjugation of RITC or TRITC with the water soluble dextran macromolecular moieties significantly enhanced their solubility (65.23 M and 149.36 M for RITC-D and TRITC-D, respectively). The higher solubility of the fluorescein dye, FITC, compared to its rhodamine counterpart, RITC, can be accounted for by the ionization of both the carboxyl and phenolic groups at pH 7.4 in addition to the smaller MW.

Results for log partition coefficient of rhodamine dyes and FITC in the isotropic n-octanol/PBS pH 7.4 system ( $\log K_{O/PBS}$ ) at 37°C ranged from -1.12 to 4.58 (Table 1) and reflected structural characteristics.  $\log K_{O/PBS}$  for Rh B was 3.42 while a lower value was obtained for Rh 110 (-0.17) despite lower solubility, owing to the lack of the two diethyl amine substituents in the xanthene ring in addition to hydrogen bonding of the primary amine group with water. A similar trend has been reported for the octanol/MES buffer pH 6.1 partition coefficient for Rh 110 compared to Rh B<sup>(32)</sup>. RITC, an isothiocyanate derivative of Rh B, expectedly exhibited a higher  $\log K_{O/PBS}$  value (4.58), attributable to hydrophobicity of the isothiocyanate substituent at the bottom of the isolated benzene ring (Figure 1). Compared to RITC, its fluorescein counterpart, FITC, was less distributed to the n-octanol phase ( $\log K_{O/PBS}$  0.85), because of its anionic nature at pH 7.4 and hydrogen bonding of the phenolic OH with water. Conjugation of either RITC or TRITC with the polar macromolecular dextran moieties, expectedly resulted in low  $\log K_{O/PBS}$  values (-1.12 and -0.60, respectively). Xanthene dyes tested can be generally ranked according to their partition in the octanol /PBS pH 7.4 system ( $\log K_{O/PBS}$ ) as follows:

$$RITC > RhB > FITC > Rh\ 110 > TRITC - D > RITC - D.$$

Log partition coefficient values of rhodamine dyes in the porcine skin / PBS pH 7.4 system ( $\log K_{S/PBS}$ ) ranged from -0.92 to 2.81. Apart from molecular characteristics, skin/ buffer partition coefficient values do reflect binding of the dyes with skin chemical constituents. Functionalization of RITC and FITC dyes with an isothiocyanate reactive group (-N=C=S), replacing a hydrogen atom on the bottom ring of the structure both increases hydrophobicity and enhances reactivity towards nucleophiles including amine and sulfhydryl groups on proteins, leading to the formation of covalent dye-protein conjugates *in vitro*<sup>(33)</sup>. Interaction of FITC with biomacromolecules near the SC of human skin has been also demonstrated by Samuelsson *et al.* 2009<sup>(34)</sup>.

A rank order correlation ( $r = 0.900$ ) was observed between  $\log K_{O/PBS}$  and  $\log K_{S/PBS}$  values (Figure 2). However, both lipophilicity parameters did not directly reflect MW or equilibrium solubility of the dyes in PBS pH 7.4 because of the diverse effects exerted by the widely different molecular characteristics. Discrepancies between solubility and partitioning behavior have been reported for various drugs<sup>(35, 36)</sup>.

## Characterization of the fabricated MN arrays

The arrays fabricated consisted of individual polymeric MNs covering an area of 0.36 cm<sup>2</sup> of the 1×1 cm<sup>2</sup> base support. Needles were conical in shape with an average basal width of 300 μm and an inter-needle spacing of 300 μm giving 11×11 arrays (121 MN/array) (Figure 3).

## *In vitro* skin permeation studies

The effect of molecular characteristics on the permeation of the test dyes through untreated and MN-treated porcine skin was the main objective of the current study. This was carried out under a given set of experimental conditions regarding the MN arrays, skin diffusional area (0.64 cm<sup>2</sup>), delivery approach (poke and patch), mode of MN application (manual), the dye solvent (PBS pH 7.4) and dye concentration (162 μM). The skin model used was basically full thickness porcine ear skin (approximately 1164 μm-thick), a well-established model representing full skin resistance and possessing characteristics similar to those of human skin<sup>(37)</sup>. Although drug saturation in the donor compartment would maximize flux, sub-saturated dye solutions (162 μM) were used in the study to avoid obstruction of microchannel pores or deposition of dye particles into the microchannels<sup>(2)</sup> and to preclude dimerization which may negatively affect dye permeation. Dye dimerization was reported to occur at dye concentrations exceeding 200 μM<sup>(38, 39)</sup>. *In vitro* skin permeation of the dyes across untreated and MN-treated porcine skin was investigated under non-occlusive conditions at pH 7.4. It should be noted that according to the determined pKa values, all dyes were in the zwitterionic form with a net neutral charge except FITC which was in the anionic form. As the experimental conditions were kept unchanged, differences in skin permeation data may be assumed to be mainly dye specific.

Passive flux of the dyes across untreated skin indicated relatively slow permeation of the two rhodamine dyes, Rh B and Rh 110 and the fluorescein dye, FITC with a lag time of approximately 6 h (Figure 4a). Permeation parameters are presented in Table 2. Rh B and Rh 110 showed more or less similar permeation profiles with no significant difference between their cumulative amount permeating at 48 h (Q<sub>48</sub>) ( $P = 0.869$ ) and steady state flux ( $P = 0.549$ ). However, FITC showed a significantly lower Q<sub>48</sub> and flux than both Rh B ( $P = 0.004$ ,  $0.001$ ) and Rh 110 ( $P = 0.001$  for both). Light microscopy image of skin penetration of Rh B is shown in Figure 5a. Data for Rh B are in accordance with those of previous reports which demonstrated accumulation of Rh B in pH 7.4 buffer in the SC of full thickness porcine ear skin and penetration into the epidermis and hair follicles<sup>(40)</sup>. Further, reported temporal imaging confirmed the penetration of Rh B into human epidermis in approximately 15 h<sup>(41)</sup>. However, porcine skin in the present study was effectively impermeable to dyes with chemical substituents capable of significantly changing the MW and physicochemical characteristics of the dyes, particularly the hydrophobic isothiocyanate group (RITC and FITC) and / or the macromolecular polar dextran moieties (RITC-D and TRITC-D). Results are consistent with the classical percutaneous absorption principles, denoting that drugs passively delivered through the skin are uncharged, small and moderately lipophilic<sup>(42)</sup>. Low passive skin flux of the isothiocyanate-substituted dyes, RITC and FITC may be explained by their potential reactivity towards skin proteins, inhibiting their transport. Reported two-photon microscopy and laser scanning confocal

microscopy imaging provided evidence for the interaction of FITC with skin biomacromolecules resulting in retention of the fluorescent dye in or adjacent to SC and preventing its intercellular transport, known to be its predominant skin permeation pathway<sup>(34)</sup>. The slightly higher flux of FITC compared to the negligible flux of RITC can be probably attributed to more favorable physicochemical characteristics, such as MW, solubility and lipophilicity (Table 1). The two macromolecular hydrophilic dyes, RITC-D and TRITC-D, were not detected in the receiver compartment owing to high MW, hydrophilicity and low partition coefficients (Table 1). It has been reported that the intercellular percutaneous absorption enhancement of the dextran-conjugated dye, FITC-D, through rat skin necessitated solubilization of SC proteins and ceramides<sup>(43, 44)</sup>.

Permeation profiles for skin samples pretreated with MN arrays indicated that, despite skin permeabilization, only transport of the dyes that passively penetrated the skin (Rh 110, Rh B and FITC) was enhanced (Figure 4b). Skin microporation resulted in a significant increase in the steady state flux of Rh 110 ( $P < 0.00005$ ), Rh B ( $P = 0.05$ ), and FITC ( $P = 0.014$ ) compared to untreated skin data. Values for permeation coefficient ( $K_p$ ) were in the order: Rh 110 > Rh B > FITC (Table 2). It is well-established that by piercing the skin with MN, a new independent interstitial fluid-filled microchannel pathway with a fractional area usually less than 1%, connects an aqueous drug vehicle to the aqueous milieu of the viable tissues in parallel with the intact skin pathway<sup>(2, 45)</sup>. This corroborates our findings regarding the three dyes. By virtue of the relative solubility of the ionic form and low MW (Table 1), the flux of these dyes probably occurs both by passive diffusion across intact skin and transport through the microchannel pathways. Simultaneous passive diffusion and infiltration of Rh B into MN-created microchannels was evidenced by light microscopy (Figure 5b). The total flux values ( $J_{TOT}$ ) were 3.6, 1.87 and 0.19  $\mu\text{g}/\text{cm}^2 \text{ h}$  for Rh 110, Rh B and FITC respectively and their calculated microchannel pathway flux ( $J_{MCP}$ ) values were 2.97, 1.06 and 0.17  $\mu\text{g}/\text{cm}^2 \text{ h}$ , respectively. The flux enhancement ratio (FER) was in the order: FITC > Rh 110 > Rh B. The high FER of FITC can be attributed to its minimal  $J_{ISP}$  value. The relative contribution of  $J_{MCP}$  and  $J_{ISP}$  to the  $J_{TOT}$  values is shown in Figure 6. Rh 110 showed the highest contribution of  $J_{MCP}$  to  $J_{TOT}$ , indicating that diffusion of Rh 110 through aqueous microchannels and its partitioning into viable tissues have been facilitated by its relatively low MW (366.80) and favourable partitioning properties,  $\log K_{O/PBS}$  (-0.17) and  $\log K_{S/PBS}$  PC (-0.5).

On the other hand, despite bypassing the SC, a potential site for isothiocyanate-protein interaction, RITC, RITC-D and TRITC-D failed to diffuse through MN-created aqueous microchannels and/or traverse viable tissues under the study conditions to reach the receiver solution for the 48 h-study period. Unfavorable molecular properties including insolubility and high partitioning parameters of RITC and relatively large MW and hydrodynamic radius of the dextran derivatives account for hindered diffusibility. Moreover, the lengthy permeation pathway through the full thickness skin, might also contribute to the poor skin permeation of the dyes<sup>(2)</sup>.

In this study, MN of 600  $\mu\text{m}$  length were used and viable tissues of full thickness porcine skin were anticipated to present greater diffusional resistance compared to the length of MN-created microchannels. To rule out the influence of diffusion path length, full thickness pig

ear skin (1164  $\mu\text{m}$ ) was replaced by dermatomed human skin (DHS, 330  $\mu\text{m}$ ) with all other parameters kept unchanged. While RITC-D and TRITC-D failed to permeate DHS, an obvious increase in RITC flux (4.99  $\mu\text{g}/\text{cm}^2\text{h}$ ) was observed (Figure 7). Apart from decreasing the diffusional path length, a possible explanation would be the lower distribution of human skin surface lipids (60.5  $\mu\text{g}/\text{cm}^2$ ) compared to porcine skin (130  $\mu\text{g}/\text{cm}^2$ )<sup>(46)</sup> allowing less binding to the lipophilic RITC. However, the skin thickness assumption cannot be adopted to explain lack of permeation of RITC-D and TRITC-D. Impermeability of DHS to RITC-D and TRITC-D under the study conditions indicated that for bulky permeants, structural characteristics and hydrodynamic radius are primary determinants of skin diffusion. In fact, permeation of macromolecules such as bovine serum albumin<sup>(47)</sup>, human IgG<sup>(48)</sup>, ovalbumin<sup>(49)</sup>, antisense oligonucleotides<sup>(50)</sup>, and plasmid DNA<sup>(51)</sup> through microporated skin could be only achieved by optimizing MN array treatment in terms of delivery approach<sup>(48, 49)</sup>, area of arrays<sup>(49)</sup> or experimental permeation conditions, including increasing drug concentration in the donor compartment<sup>(48)</sup>, diffusion area<sup>(47)</sup> and application force<sup>(12, 47)</sup> or reducing diffusional path length by using dermatomed skin<sup>(12)</sup> or heat separated epidermis<sup>(47)</sup>. Furthermore, a combined skin permeation enhancement approach including both MN treatment and physical enhancement methods such as iontophoresis<sup>(50, 52)</sup> and in-skin electroporation<sup>(53)</sup> has been reported for more effective transdermal delivery of macromolecules.

Finally, it was also of interest to assess the influence of the prototropic form of rhodamine dyes on permeation through MN-treated skin using Rh B as a model. This was achieved by comparing permeation data at pH 7.4 where Rh B exists predominantly in the zwitterionic form with neutral net charge to those obtained at pH 3.2 where the cationic form predominates<sup>(54)</sup>. Data is shown in Table 2. Transport of the less hydrophilic zwitterionic Rh B across MN treated porcine skin was faster than the charged species although the difference in  $Q_{48}$  and flux did not reach statistical significance ( $P = 0.357$  and  $0.381$  for flux and  $Q_{48}$ , respectively). This indicates that diffusion of Rh B across microporated skin was not significantly affected by its prototropic form. FER was higher for the charged Rh B compared to the zwitterionic form (2.69 and 1.37 for cationic and zwitterionic Rh B respectively), suggesting greater selectivity of the charged form of the dye to diffuse through the microchannels than through intact skin around the microchannels. Similarly, a larger FER for the more soluble charged naltrexol relative to its unionized form has been demonstrated by Banks *et al.*<sup>(11)</sup> after MN-treatment of full thickness human and guinea pig skin.

## CONCLUSION

*In vitro* skin permeation of a series of structurally related ionic xanthene dyes across MN-treated full thickness porcine skin was assessed in relation to the passive diffusion of the dyes through intact skin and their molecular characteristics. It was appreciated at the outset that an individual physicochemical property cannot be addressed separately from other properties in interpreting effects on skin permeation. Although aqueous solubility / hydrophilicity of the permeant are important parameters for permeation through MN-created aqueous conduits, these could be overridden by the molecular weight and structural characteristics hindering diffusivity through the conduits and subsequent viable tissue layers.

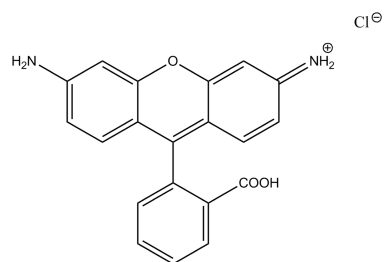
This was obvious for a chemical substituent with binding potential toward SC proteins and a macromolecular substituent. Further, flux across MN-created microchannels was not significantly affected by the ionic form of a water soluble dye, Rh B while its partition coefficient was important for passive diffusion which contributed to the total flux. It is worth noting that for a valid comparison of skin permeation data, findings of studies on MN-assisted permeation of high MW drugs cannot be adopted without taking in consideration experimental variables such as skin model, MN type, application force and the use of additional enhancement methods. In the wider context, findings of this study are useful for a more rational design of both MN-based effective transdermal delivery systems and *in vitro* skin permeation experiments for research purposes.

## References

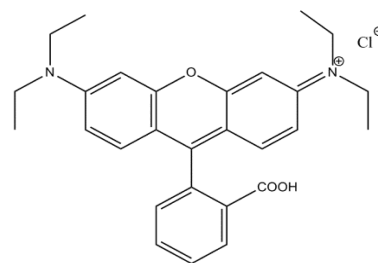
1. Donnelly, RF.; Singh, TRR.; Morrow, DIJ.; Woolfson, AD. Microneedle-mediated transdermal and intradermal drug delivery. John Wiley & Sons, Ltd; Oxford, UK: 2012.
2. Milewski M, Stinchcomb AL. Vehicle composition influence on the microneedle-enhanced transdermal flux of naltrexone hydrochloride. *Pharm Res.* 2011; 28(1):124–134. [PubMed: 20577787]
3. Guy RH, Hadgraft J. Physicochemical aspects of percutaneous penetration and its enhancement. *Pharm Res.* 1988; 5(12):753–8. [PubMed: 3247284]
4. Bariya SH, Gohel MC, Mehta TA, Sharma OP. Microneedles: an emerging transdermal drug delivery system. *J Pharm Pharmacol.* 2012; 64(1):11–29. [PubMed: 22150668]
5. Teo MA, Shearwood C, Ng KC, Lu J, Moochhala S. In vitro and in vivo characterization of MEMS microneedles. *Biomed Microdevices.* 2005; 7(1):47–52. [PubMed: 15834520]
6. Chu LY, Prausnitz MR. Separable arrowhead microneedles. *J Control Rel.* 2011; 149(3):242–249.
7. Kalluri H, Banga AK. Formation and closure of microchannels in skin following microporation. *Pharm Res.* 2011; 28(1):82–94. [PubMed: 20354766]
8. Garland, MJ.; Migalska, K.; Mahmood, T.; Woolfson, D.; Caffarel-Salvador, E.; Majithiya, R.; McCrudden, C.; McCarthy, H.; Donnelly, RF. Choice of skin model is important in predicting performance of drug loaded soluble microneedle arrays. Queen's University Belfast; Belfast:
9. Donnelly RF, Garland MJ, Morrow DIJ, Migalska K, Singh TRR, Majithiya R, Woolfson AD. Optical coherence tomography is a valuable tool in the study of the effects of microneedle geometry on skin penetration characteristics and in-skin dissolution. *J Control Release.* 2010; 147(3):333–341. [PubMed: 20727929]
10. McAllister DV, Wang PM, Davis SP, Park JH, Canatella PJ, Allen MG, Prausnitz MR. Microfabricated needles for transdermal delivery of macromolecules and nanoparticles: fabrication methods and transport studies. *Proc Natl Acad Sci USA.* 2003; 100(24):13755–60. [PubMed: 14623977]
11. Banks SL, Pinninti RR, Gill HS, Crooks PA, Prausnitz MR, Stinchcomb AL. Flux across of microneedle-treated skin is increased by increasing charge of Naltrexone and Naltrexol in vitro. *Pharm Res.* 2008; 25(7):1677–1685. [PubMed: 18449628]
12. Verbaan FJ, Bal SM, van den Berg DJ, Groenink WH, Verpoorten H, Luttge R, Bouwstra JA. Assembled microneedle arrays enhance the transport of compounds varying over a large range of molecular weight across human dermatomed skin. *J Control Release.* 2007; 117(2):238–245. [PubMed: 17196697]
13. Qiu Y, Gao Y, Hu K, Li F. Enhancement of skin permeation of docetaxel: a novel approach combining microneedle and elastic liposomes. *J Control Release.* 2008; 129(2):144–150. [PubMed: 18538885]
14. Coulman SA, Anstey A, Gateley C, Morrissey A, McLoughlin P, Allender C, Birchall JC. Microneedle mediated delivery of nanoparticles into human skin. *Int J Pharm.* 2009; 366(1-2): 190–200. [PubMed: 18812218]

15. Zhang W, Gao J, Zhu Q, Zhang M, Ding X, Wang X, Hou X, Fan W, Ding B, Wu X, Gao S. Penetration and distribution of PLGA nanoparticles in the human skin treated with microneedles. *Int J Pharm.* 2010; 402(1-2):205–212. [PubMed: 20932886]
16. Shkilnyy A, Proulx P, Sharp J, Lepage M, Vermette P. Diffusion of rhodamine B and bovine serum albumin in fibrin gels seeded with primary endothelial cells. *Colloids Surf B Biointerfaces.* 2012; 93:202–207. [PubMed: 22293601]
17. Hilderbrand SA, Weissleder R. One-pot synthesis of new symmetric and asymmetric xanthene dyes. *Tetrahedron Lett.* 2007; 48(25):4383–4385. [PubMed: 19834587]
18. Kuchler S, Abdel-Mottaleb M, Lamprecht A, Radowski MR, Haag R, Schafer-Korting M. Influence of nanocarrier type and size on skin delivery of hydrophilic agents. *Int J Pharm.* 2009; 377(1-2):169–172. [PubMed: 19439166]
19. Avdeef A, Box KJ, Comer JE, Gilges M, Hadley M, Hibbert C, Patterson W, Tam KY. PH-metric log P 11. pKa determination of water-insoluble drugs in organic solvent-water mixtures. *J Pharm Biomed Anal.* 1999; 20(4):631–41. [PubMed: 10704132]
20. Eirkson, C.; Harrass, MC.; Osbourne, CM.; Sayre, PG.; Zeeman, M. Environmental assessment technical assistance handbook 3.01 PB87–175345 U.S. Food and Drug Administration. Washington DC: 1987. Water solubility; p. 1-11.
21. Chiang CH, Lai JS, Yang KH. The effect of pH and chemical enhancers on the percutaneous absorption of indomethacin. *Drug Dev Ind Pharm.* 1991; 17(1):91–111.
22. Tojo K, Chiang CC, Chien YW. Drug permeation across the skin: effect of penetrant hydrophilicity. *J Pharm Sci.* 1987; 76(2):123–6. [PubMed: 3572749]
23. Saket MM, James KC, Kellaway IW. Partitioning of some 21 alkyl esters of hydrocortisone and cortisone. *Int J Pharm.* 1984; 21(2):155–166.
24. Gomaa YA, Morrow DI, Garland MJ, Donnelly RF, El-Khordagui LK, Meidan VM. Effects of microneedle length, density, insertion time and multiple applications on human skin barrier function: assessments by transepidermal water loss. *Toxicol In Vitro.* 2010; 24(7):1971–1978. [PubMed: 20732409]
25. Kretsos K, Kasting GB. A geometrical model of dermal capillary clearance. *Math Biosci.* 2007; 208(2):430–453. [PubMed: 17303187]
26. Alvarez-Roman R, Naik A, Kalia YN, Guy RH, Fessi H. Skin penetration and distribution of polymeric nanoparticles. *J Control Release.* 2004; 99(1):53–62. [PubMed: 15342180]
27. Fischer H, Kansy M, Avdeef A, Senner F. Permeation of permanently positive charged molecules through artificial membranes—Influence of physico-chemical properties. *Eur J Pharm Sci.* 2007; 31(1):32–42. [PubMed: 17416489]
28. Jeannot V, Salmon JM, Deumie M, Viallet P. Intracellular accumulation of rhodamine 110 in single living cells. *J Histochem Cytochem.* 1997; 45(3):403–412. [PubMed: 9071322]
29. Woislowski S. The spectrophotometric determination of ionization constants of basic dyes. *J Am Chem Soc.* 1953; 75(21):5201–5203.
30. Hii S-L, Yong S-Y, Wong C-L. Removal of rhodamine B from aqueous solution by sorption on *Turbinaria conoides* (Phaeophyta). *J Appl Phycol.* 2009; 21:625–631.
31. Boonacker E, Van Noorden CJ. Enzyme cytochemical techniques for metabolic mapping in living cells, with special reference to proteolysis. *J Histochem Cytochem.* 2001; 49(12):1473–1486. [PubMed: 11724895]
32. Tansil NC, Li Y, Koh LD, Peng TC, Win KY, Liu XY, Han M-Y. The use of molecular fluorescent markers to monitor absorption and distribution of xenobiotics in a silkworm model. *Biomaterials.* 2011; 32:9576–9583. [PubMed: 21955689]
33. Brinkley M. A brief survey of methods for preparing protein conjugates with dyes, haptens, and cross-linking reagents. *Bioconjug Chem.* 1992; 3(1):2–13. [PubMed: 1616945]
34. Samuelsson K, Simonsson C, Jonsson CA, Westman G, Ericson MB, Karlberg AT. Accumulation of FITC near stratum corneum-visualizing epidermal distribution of a strong sensitizer using two-photon microscopy. *Contact Dermatitis.* 2009; 61(2):91–100. [PubMed: 19706049]
35. Kwon JW, Armbrust KL. Aqueous solubility, n-octanol-water partition coefficient, and sorption of five selective serotonin reuptake inhibitors to sediments and soils. *Bull Environ Contam Toxicol.* 2008; 81(2):128–35. [PubMed: 18389163]

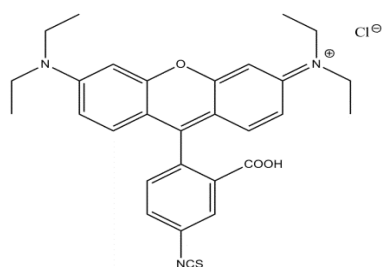
36. Ueda H, Sugibayashi K, Morimoto Y. Skin penetration-enhancing effect of drugs by phonophoresis. *J Control Release*. 1995; 37(3):291–297.
37. Caon T, Costa ACO, Leal de Oliveirac MA, Micke GA, Simões CMO. Evaluation of the transdermal permeation of different paraben combinations through a pig ear skin model. *Int J Pharm*. 2010; 391(1):1–6. [PubMed: 20156540]
38. Tajalli H, Ghanadzadeh Gilani A, Zakerhamidi MS, Moghadam M. Effects of surfactants on the molecular aggregation of rhodamine dyes in aqueous solutions. *Spectrochim Acta A Mol Biomol Spectrosc*. 2009; 72(4):697–702. [PubMed: 19147398]
39. Zhao X, Zhou S, Chen M, Wu L. Supramolecular architecture, spectroscopic properties and stability of C.I. Basic Violet 10 (Rhodamine B) at high concentration. *Dyes and Pigments*. 2009; 80(2):212–218.
40. Gillet A, Lecomte F, Hubert P, Ducat E, Evrard B, Piel G. Skin penetration behaviour of liposomes as a function of their composition. *Eur J Pharm Biopharm*. 2011; 79(1):43–53. [PubMed: 21272638]
41. Simonsson C, Smedh M, Jonsson C, Ericson MB. Temporal imaging chamber (TIC) for en face imaging of epidermal absorption in vitro. *Proc. SPIE*. 2009; 7367:73671H1–73671H7.
42. Prausnitz MR, Langer R. Transdermal drug delivery. *Nat Biotechnol*. 2008; 26(11):1261–1268. [PubMed: 18997767]
43. Ogiso T, Paku T, Iwaki M, Tanino T. Percutaneous penetration of fluorescein isothiocyanate-dextrans and the mechanism for enhancement effect of enhancers on the intercellular penetration. *Biol Pharm Bull*. 1995; 18(11):1566–1571. [PubMed: 8593481]
44. Ogiso T, Paku T, Iwaki M, Tanino T. Mechanism of the enhancement effect of n-octyl-beta-D-thioglucoiside on the transdermal penetration of fluorescein isothiocyanate-labeled dextrans and the molecular weight dependence of water-soluble penetrants through stripped skin. *J Pharm Sci*. 1994; 83(12):1676–1681. [PubMed: 7534349]
45. Milewski M, Brogden NK, Stinchcomb AL. Current aspects of formulation efforts and pore lifetime related to microneedle treatment of skin. *Expert Opin Drug Deliv*. 2010; 7(5):617–29. [PubMed: 20205604]
46. Walters, KA.; Roberts, MS. Veterinary applications of skin penetration enhancers. In: Walters, KA.; Hadgraft, J., editors. *Pharmaceutical skin penetration enhancement*. Marcel Dekker; New York: 1993.
47. Park JH, Allen MG, Prausnitz MR. Biodegradable polymer microneedles: fabrication, mechanics and transdermal drug delivery. *J Control Release*. 2005; 104(1):51–66. [PubMed: 15866334]
48. Li G, Badkar A, Nema S, Kolli CS, Banga AK. In vitro transdermal delivery of therapeutic antibodies using maltose microneedles. *Int J Pharm*. 2009; 368(1-2):109–115. [PubMed: 18996461]
49. Matriano JA, Cormier M, Johnson J, Young WA, Buttery M, Nyam K, Daddona PE. Macroflux microprojection array patch technology: a new and efficient approach for intracutaneous immunization. *Pharm Res*. 2002; 19(1):63–70. [PubMed: 11837701]
50. Lin W, Cormier M, Samiee A, Griffin A, Johnson B, Teng CL, Hardee GE, Daddona PE. Transdermal delivery of antisense oligonucleotides with microprojection patch (Macroflux) technology. *Pharm Res*. 2001; 18(12):1789–93. [PubMed: 11785702]
51. Mikszta JA, Alarcon JB, Brittingham JM, Sutter DE, Pettis RJ, Harvey NG. Improved genetic immunization via micromechanical disruption of skin-barrier function and targeted epidermal delivery. *Nat Med*. 2002; 8(4):415–9. [PubMed: 11927950]
52. Wu XM, Todo H, Sugibayashi K. Enhancement of skin permeation of high molecular compounds by a combination of microneedle pretreatment and iontophoresis. *J Control Release*. 2007; 118(2): 189–195. [PubMed: 17270306]
53. Yan K, Todo H, Sugibayashi K. Transdermal drug delivery by in-skin electroporation using a microneedle array. *Int J Pharm*. 2010; 397(1-2):77–83. [PubMed: 20619329]
54. Ghasemi J, Niazi A, Kubista M. Thermodynamics study of the dimerization equilibria of rhodamine B and 6G in different ionic strengths by photometric titration and chemometrics method. *Spectrochim Acta A Mol Biomol Spectrosc*. 2005; 62(1-3):649–56. [PubMed: 16257772]



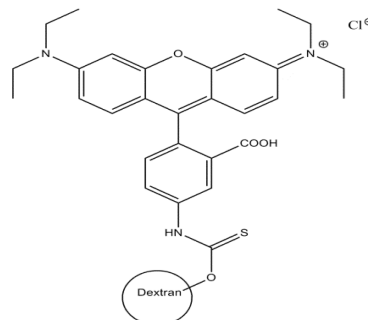
Rhodamine 110  
(Rh 110)



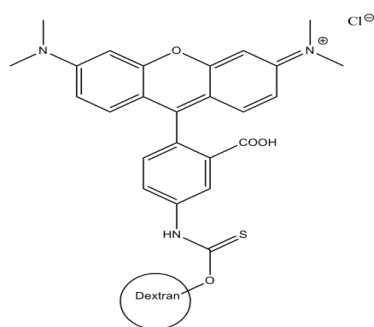
Rhodamine B  
(Rh B)



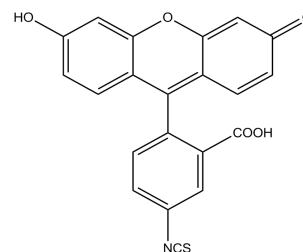
Rhodamine isothiocyanate  
(RITC)



Rhodamine isothiocyanate dextran  
(RITC-D)



Tetramethylrhodamine isothiocyanate dextran  
(TRITC-D)



Fluorescein isothiocyanate  
(FITC)

**Figure 1. Chemical structures of the six xanthene dyes.**

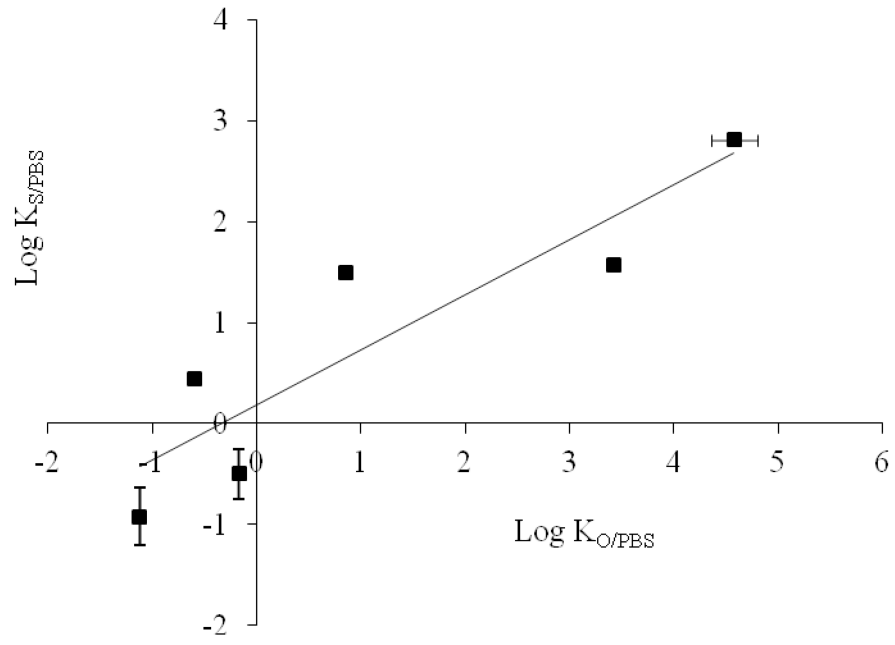


**Figure 2. Relation between Log K<sub>O</sub>/PBS and Log K<sub>S</sub>/PBS of the test dyes.**  
Error bars represent SD values; with n = 3.

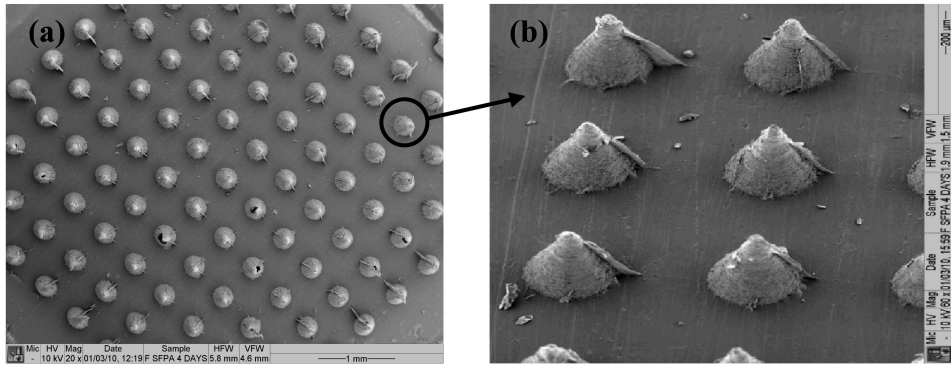


**Figure 3.** SEM images showing top (a) and side (b) views of solid MN arrays (600  $\mu\text{m}$ -long and 121 MN/array dense).

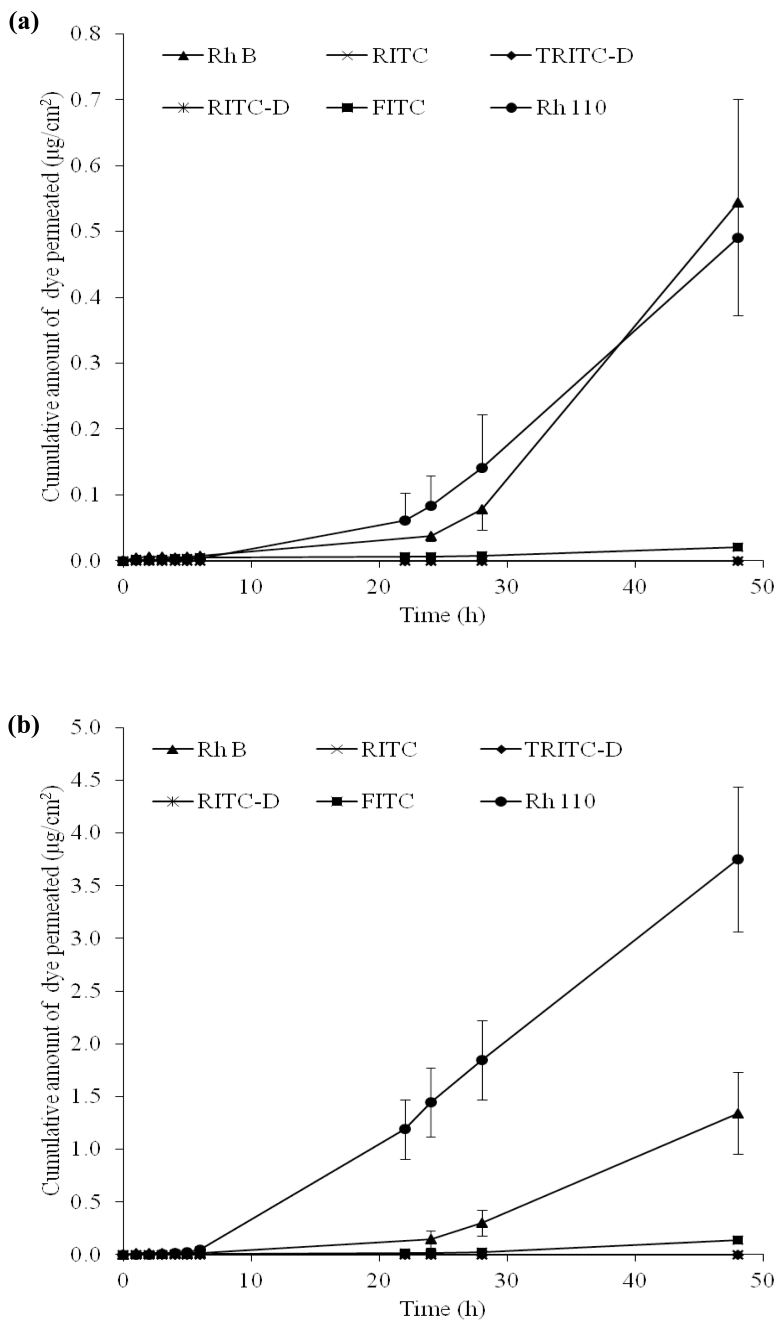


**Figure 4. Permeation profiles of the test dyes through (a) untreated porcine skin and (b) MN-treated porcine skin.**

Error bars represent SD values; with n = 3.

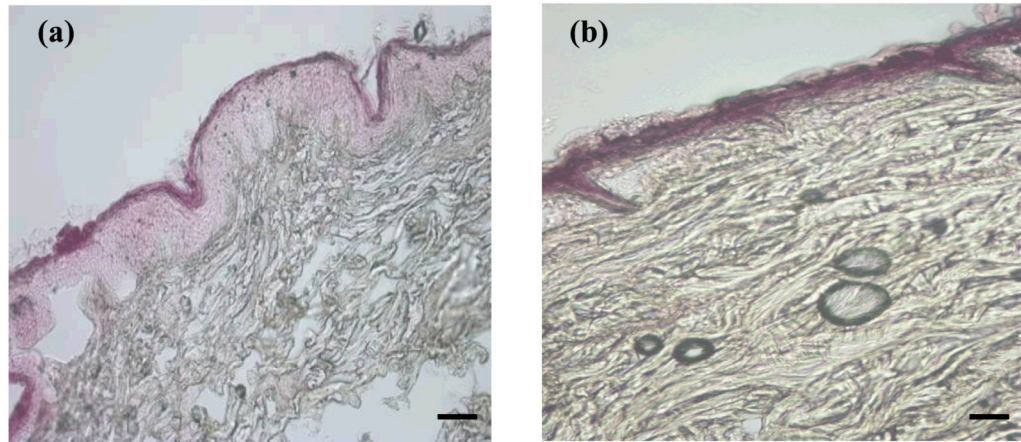


**Figure 5. Light microscopy images showing vertical sections of porcine skin, control (a), MN-pretreated skin (b) treated with Rh B dye solution.**  
Bar scales represent 100 µm.

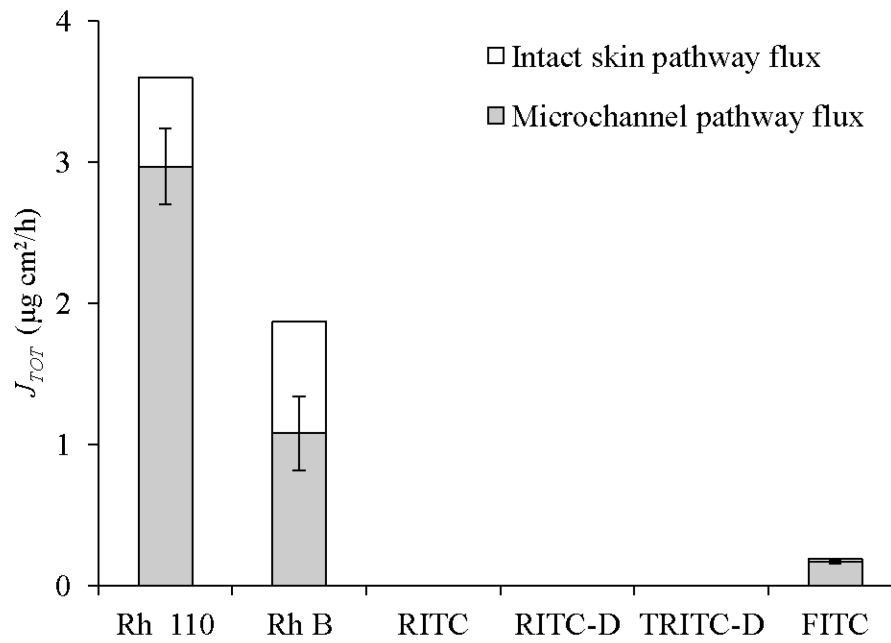


**Figure 6.** Relative contribution of microchannel pathway flux ( $J_{MCP}$ ) and intact skin pathway flux ( $J_{ISP}$ ) to the total transdermal flux ( $J_{TOT}$ ) of dyes through full thickness porcine skin. Error bars represent SD values; with  $n = 3$ .

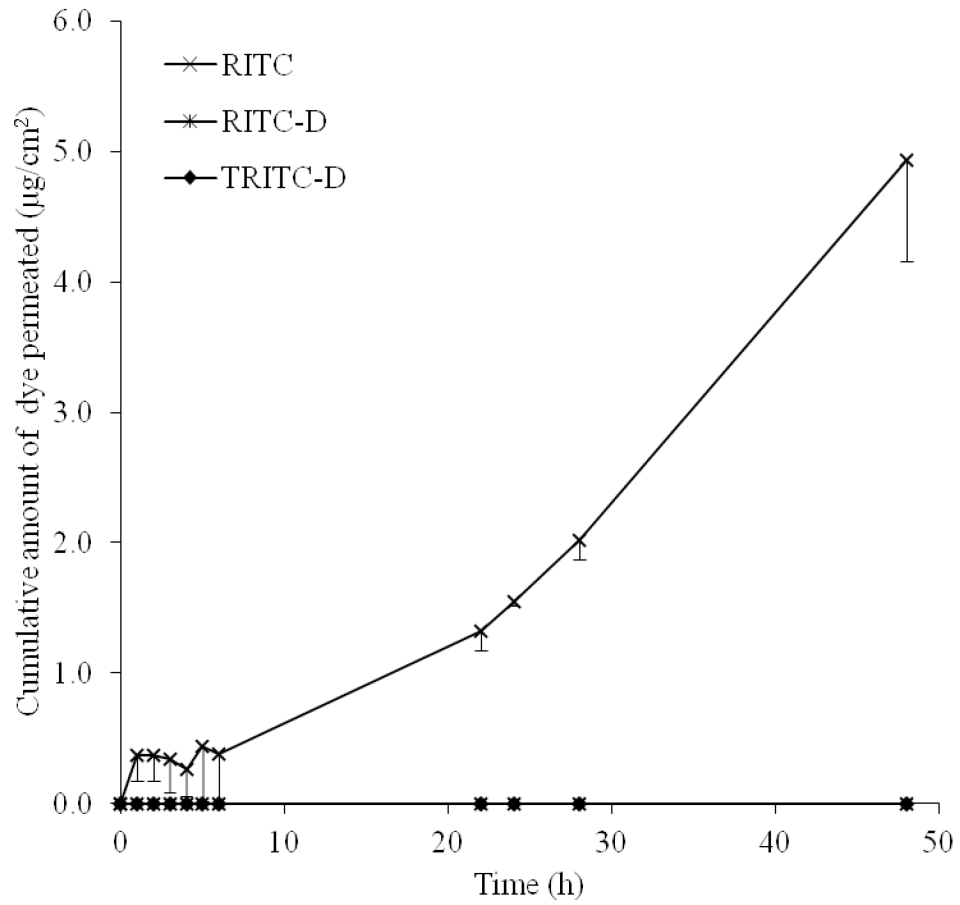


**Figure 7.** The permeation profile of RITC, RITC-D and TRIC-D through MN-pre-treated DHS. Error bars represent SD values; with n = 3.

**Table 1**  
**Physicochemical characteristics of the dyes under study.**

Values are average  $\pm$  SD (n = 3).

Dye	MW (Da)	pKa <sup>1</sup>	Solubility <sup>2</sup> (M)	pH <sup>3</sup>	Log K <sub>O/PBS</sub> <sup>4</sup>	Log K <sub>S/PBS</sub> <sup>5</sup>
Rh 110	366.80	3.48 $\pm$ 0.05	0.06 $\pm$ 0.00	7.49	-0.17 $\pm$ 0.03	-0.50 $\pm$ 0.25
Rh B	479.02	3.25 $\pm$ 0.40	0.99 $\pm$ 0.08	7.39	3.42 $\pm$ 0.06	1.57 $\pm$ 0.01
RITC	538.08	3.68 $\pm$ 0.65	Practically insoluble	7.47	4.58 $\pm$ 0.22	2.81 $\pm$ 0.01
RITC-D	10000	3.31 $\pm$ 0.03	65.23 $\pm$ 2.91	7.52	-1.12 $\pm$ 0.04	-0.92 $\pm$ 0.28
TRITC-D	4400	3.97 $\pm$ 0.01	149.36 $\pm$ 13.18	7.53	-0.60 $\pm$ 0.01	0.44 $\pm$ 0.03
FITC	389.38	4.06 $\pm$ 0.24 6.20 $\pm$ 0.04	0.09 $\pm$ 0.01	7.34	0.85 $\pm$ 0.01	1.50 $\pm$ 0.05

<sup>1</sup> dissociation constant determined potentiometrically at 25°C

<sup>2</sup> Solubility in PBS (pH 7.4) at 37°C

<sup>3</sup> pH of 162  $\mu$ M dye solution in PBS (pH 7.4)

<sup>4</sup> n-Octanol/PBS partition coefficient at 37°C

<sup>5</sup> Porcine skin/PBS partition coefficient at 37°C

**Table 2**  
**Permeation parameters of the dyes through full thickness porcine skin at pH 7.4.**

Values are average  $\pm$  SD (n = 3).

Dye	Total		Intact skin pathway		Microchannel pathway		$K_p^1$ (x <sup>3</sup> h/cm10)	FER <sup>2</sup>
	Q <sub>48</sub> (µg/cm <sup>2</sup> )	Flux ( µg/cm <sup>2</sup> h )	Q <sub>48</sub> (µg/cm <sup>2</sup> )	Flux ( µg/cm <sup>2</sup> h )	Q <sub>48</sub> (µg/cm <sup>2</sup> )	Flux ( µg/cm <sup>2</sup> h )		
Rh 110	3.75 $\pm$ 0.69	3.60 $\pm$ 0.88	0.49 $\pm$ 0.21	0.63 $\pm$ 0.27	3.26	2.97	50.08	4.71
Rh B	1.34 $\pm$ 0.39	1.87 $\pm$ 0.57	0.54 $\pm$ 0.17	0.79 $\pm$ 0.26	0.8	1.08	13.94	1.37
Rh B (pH 3.2)	1.15 $\pm$ 0.39	1.66 $\pm$ 0.53	0.32 $\pm$ 0.12	0.45 $\pm$ 0.16	0.83	1.21	15.61	2.69
RITC	-	-	-	-	-	-	-	-
RITC-D	-	-	-	-	-	-	-	-
TRITC-D	-	-	-	-	-	-	-	-
FITC	0.14 $\pm$ 0.02	0.19 $\pm$ 0.03	0.02 $\pm$ 0.01	0.02 $\pm$ 0.01	0.12	0.17	2.70	8.50

-: Not detected

<sup>1</sup> permeability coefficient,  $J_{MCP}$  / initial donor concentration

<sup>2</sup> Flux Enhancement ratio,  $J_{MCP} / J_{ISP}$